6-2012

# The Clustering of Ha Emitters at z=2.23 from HiZELS

J. E. Geach
*McGill University*

D. Sobral
*Leiden University*

R. C. Hickox
*Dartmouth College*

D. A. Wake
*Yale University*

# The clustering of Hα emitters at z = 2.23 from HiZELS

J. E. Geach,[1][*] D. Sobral[2], R. C. Hickox[3], D. A. Wake[4], Ian Smail[5], P. N. Best[6], C. M. Baugh[5] and J. P. Stott[5]

[1]*Department of Physics, McGill University, 3600 Rue University, Montréal, Québec, H3A 2T8, Canada*
[2]*Leiden Observatory, Leiden University, P.O. Box 9513, NL–2300 RA Leiden, The Netherlands*
[3]*Department of Physics and Astronomy, Dartmouth College, 6127 Wilder Laboratory, Hanover, NH 03755, USA*
[4]*Department of Astronomy, Yale University, New Haven, CT 06520, USA*
[5]*Institute for Computational Cosmology, Department of Physics, Durham University, South Road, Durham, DH1 3LE, UK*
[6]*SUPA, Institute for Astronomy, Royal Observatory of Edinburgh, Blackford Hill, Edinburgh, EH9 3HJ, UK*

**ABSTRACT**

We present a clustering analysis of 370 high-confidence Hα emitters (HAEs) at $z = 2.23$. The HAEs are detected in the Hi-Z Emission Line Survey (HiZELS), a large-area blank field $2.121\,\mu$m narrowband survey using the United Kingdom Infrared Telescope (UKIRT) Wide Field Camera (WFCAM). Averaging the two-point correlation function of HAEs in two ∼1 degree scale fields (United Kingdom Infrared Deep Sky Survey/Ultra Deep Survey [UDS] and Cosmological Evolution Survey [COSMOS] fields) we find a clustering amplitude equivalent to a correlation length of $r_0 = 3.7 \pm 0.3\,h^{-1}$ Mpc for galaxies with star formation rates of $\gtrsim 7\,M_\odot\,\mathrm{yr}^{-1}$. The data are well-fitted by the expected correlation function of Cold Dark Matter, scaled by a bias factor: $\omega_{\mathrm{HAE}} = b^2\omega_{\mathrm{DM}}$ where $b = 2.4^{+0.1}_{-0.2}$. The corresponding 'characteristic' mass for the halos hosting HAEs is $\log(M_{\mathrm{h}}/[h^{-1}M_\odot]) = 11.7 \pm 0.1$. Comparing to the latest semi-analytic GALFORM predictions for the evolution of HAEs in a ΛCDM cosmology, we find broad agreement with the observations, with GALFORM predicting a HAE correlation length of $\sim 4\,h^{-1}$ Mpc. Motivated by this agreement, we exploit the simulations to construct a parametric model of the halo occupation distribution (HOD) of HAEs, and use this to fit the observed clustering. Our best-fitting HOD can adequately reproduce the observed angular clustering of HAEs, yielding an effective halo mass and bias in agreement with that derived from the scaled $\omega_{\mathrm{DM}}$ fit, but with the relatively small sample size the current data provide a poor constraint on the HOD. However, we argue that this approach provides interesting hints into the nature of the relationship between star-forming galaxies and the matter field, including insights into the efficiency of star formation in massive halos. Our results support the broad picture that 'typical' ($\lesssim L^\star$) star-forming galaxies have been hosted by dark matter haloes with $M_{\mathrm{h}} \lesssim 10^{12}h^{-1}M_\odot$ since $z \approx 2$, but with a broad occupation distribution and clustering that is likely to be a strong function of luminosity.

**Key words:** galaxies: evolution, high-redshift, star-forming

## 1 INTRODUCTION

The Cold Dark Matter model contends that galaxies are biased tracers of an unseen, underlying cold dark matter distribution that has evolved from primordial fluctuations into a rich hierarchy of structure, with baryons forming into galaxies within gravitationally bound dark matter halos (White & Rees 1978). Understanding the relationship between the distribution of observed galaxies, their properties, and their co-evolution with the latent matter field is a key question of observational cosmology, and can yield important information about a galaxy population (Peebles 1980).

One of the simplest, but also the most powerful, tools at our disposal to address this issue is the clustering of galaxies, as has been recognised for many years (Rubin 1954; Groth & Peebles 1977; Peebles 1980). At a basic level, the statistics of counts of galaxy pairs, relative to random distributions, reveal the scales over which the fluctuations in the spatial distribution of galaxies are correlated, and therefore a measure of how 'clustered' a population is; longer correlation lengths correspond to stronger clustering and an indication that those galaxies are hosted by, on average, more biased and hence more massive dark matter halos (e.g. Mo & White 1996).

In the local Universe, mature wide-area surveys such as the Sloan Digital Sky Survey (SDSS; York et al. 2000) and the Two De-

gree Field (2dF) Redshift Survey (Colless et al. 2001), have delivered highly accurate measurements of the clustering of populations of galaxies and quasars (Norberg et al. 2001; Myers et al. 2006; Ross et al. 2009; Wake et al. 2008; Zehavi et al. 2011). A key result of these studies is the observation that the clustering amplitude is enhanced as the mass limit of the galaxy sample increases, indicating that the more massive galaxies are hosted by more massive halos. Furthermore, it is clear that *passive* galaxies are more strongly clustered on small spatial scales compared to galaxies with ongoing star formation (e.g. Norberg et al. 2002). Over the past decade a method of interpreting these observations has been developed (in part motivated by large *N*-body simulations) which expresses the distribution of galaxies relative to the matter field through a probabilistic halo occupation distribution (HOD; Benson et al. 2000; Cooray & Sheth 2002; Zheng et al. 2005) or, similarly, a conditional luminosity function (Yang et al. 2003). Halo models provide an intuitive framework to relate observed projected correlation functions to the hierarchical paradigm, and are becoming increasingly common tools for the interpretation of clustering data.

Clustering analyses are now routine for high redshift ($z > 1$) mass-limited galaxy samples, largely thanks to the increased efficiency of deep and wide-area ($\sim$1 degree scale) multi-band (ultraviolet–optical–near-infrared) imaging surveys offering excellent photometric redshifts (accurate to the few percent level at $z \sim 1$) and stellar mass estimates for large numbers of massive galaxies (e.g. Wake et al. 2011). When it comes to measuring the clustering properties of purely star-forming galaxies at high redshifts, which – in the halo model context – could yield important clues about the environmental trends in the history of stellar mass assembly, the main challenge is to understand the selection function, since most broad-band selections (Lyman Break, BX/BM, 'sBzK', and so-on) can result in heterogeneous samples with broad redshift distributions, and can be biased towards stellar mass in complicated ways. The latter two issues are undesirable, given the strong evolution in the specific star formation rates (SFRs) of galaxies since $z \sim 1$–2 (Noeske et al. 2007; Elbaz et al. 2011).

Narrowband ($\Delta\lambda/\lambda \simeq 10^{-3}$) selections of star-forming galaxies are of great value in this regard, as they allow for the clean selection of galaxies based simply on the strength of an emission line sampled by the filter. The narrow bandpass corresponds to a narrow redshift window, within which the population is not expected to evolve. The main contaminants to such a survey are emission-line galaxies at different redshifts corresponding to the redshifting of alternative lines into the band. For high-$z$ surveys these contaminants are predominantly lower-redshift populations and easily removed (see §2). Most narrowband-selected clustering analyses conducted so-far have targeted the Ly$\alpha$ emission line, redshifted into the optical window for $z \simeq 3$ and thus convenient for deep, wide-field surveys out to very high redshifts (e.g. Ouchi et al. 2003). The development of wide-format infrared cameras over the past decade has now cleared the way for panoramic near-infrared narrowband surveys that target the H$\alpha$ nebular line at epochs of $z \sim$1–2, spanning the peak in the global star formation rate density, and thus one of the most important intervals in galaxy formation studies. H$\alpha$ is favoured over the Ly$\alpha$ line because of its (a) weaker dust obscuration (and ease of extinction correction, if the Balmer decrement is known), (b) better understood radiative transfer compared to the resonant Ly$\alpha$ and (c) more accurate luminosity-to-star formation rate calibrations from surveys of local star forming regions. It is also important to measure the clustering of HAEs in preparation for the *Euclid* mission, as one of the probes used to

constrain the nature of dark energy will be a slitless redshift survey of HAEs (Laureijs et al. 2011).

In this paper we present a clustering analysis of H$\alpha$ emitters (HAEs) at $z = 2.23$ detected in our Hi-Z Emission Line (HiZELS) survey: a wide-field near-infrared narrowband survey selecting H$\alpha$ emitting galaxies in three narrow 'slices' of redshift at $z = 0.84$, $z = 1.47$ and $z = 2.23$ (e.g. Geach et al 2008; Best et al. 2010; Sobral et al. 2010, 2012). In §2 we provide a brief review of the observations and selection technique (although we refer the reader to the aforementioned HiZELS publications for a complete, comprehensive description); in §3 we describe the clustering analysis and present the results in §4, where we approach the interpretation of the data with a series of models of increasing sophistication, from a simple power law fit to a full halo model. In §5 we discuss our findings and conclude with a review of the main results in §6. Throughout this work we quote magnitudes on the AB system, and assume a cosmology with $\Omega_{\mathrm{m}} = 0.27$, $\Omega_{\Lambda} = 0.73$, $\sigma_8 = 0.8$ and $H_0 = 100h \,\mathrm{km\,s^{-1}\,Mpc^{-1}}$ with $h = 0.7$. The co-moving distance to $z = 2.23$ is 5128 Mpc in this cosmology.

## 2    NARROWBAND SELECTION OF H$\alpha$ EMITTERS

The observations and selection of HAEs in the primary HiZELS fields of the United Kingdom Infrared Deep Sky Survey (UKIDSS) Ultra Deep Survey (UDS; Lawrence et al. 2007) and Cosmological Evolution Survey (COSMOS; Scoville et al. 2007) are described in more detail by Sobral et al. (2012) – we refer the reader to that article for a comprehensive overview of the selection technique, but in short we first select galaxies based on the significance of their 'colour excess' in the narrow band. Corrections to the continuum slope over the bandpass of the $K$-band filter (which could mimic a colour excess) is performed by interpolating over the neighbouring broad band (in this case, the $H$-band). Further broad band colour selections are performed to refine the selection (which can be contaminated by lower redshift Paschen and Brackett lines for example). Here we perform a flux cut to obtain a catalogue of approximately uniform depth across both UDS and COSMOS fields.

The flux limit at which we are uniformly complete to >50% over both UDS and COSMOS fields is $f_{\mathrm{H}\alpha} = 5 \times 10^{-17} \,\mathrm{erg\,s^{-1}\,cm^{-2}}$, corresponding to a luminosity of $\log_{10}(L_{\mathrm{H}\alpha}/\mathrm{erg\,s^{-1}}) = 42.3$ at $z = 2.23$. Note that variations in the exact depth of each WFCAM pointing (each field is a mosaic of several pointings) corresponds to a variation in the surface density of galaxies. The impact of this on our measured clustering is in part absorbed into the error bars calculated by jackknife resampling of the survey area that we describe in §3.2. Assuming a $L_{\mathrm{H}\alpha}$–SFR calibration of $1.3 \times 10^{41} \,\mathrm{erg\,s^{-1}}$ per $M_{\odot}\,\mathrm{yr^{-1}}$ (Kennicutt et al. 1998), our selection is SFR limited at $\geqslant 7 \, M_{\odot}\,\mathrm{yr^{-1}}$ assuming a canonical 1 mag of extinction in the H$\alpha$ line. Foreground sources are easily removed by high-quality photometric redshifts estimated from UV–optical–near-infrared photometry in both the UDS and COSMOS fields. Sobral et al. (2012) present the $z_{\mathrm{phot}}$ distribution for $K$-band selected HAEs, indicating the most significant peak in the distribution at $z = 2.23$, but with low-redshift enhancements at the expected wavelengths of Pa$\alpha$, Pa$\beta$, He I, [S III], and at high redshift [O III] at $z \sim 3.3$.

To refine the photometric selection, we make use of a key design feature of HiZELS, namely the fact that our custom-made $J$ and $H$-band narrow-band filters select [O II] and [O III] emitters at $z = 2.23$ respectively. Thus, double or triple detections for the same source in each of the narrow-bands provides an extremely ro-

bust selection with almost no contamination. There are 84 $z = 2.23$ HiZELS sources detected in this way, and this is used to refine photometric redshift cuts and broad-band photometric selections as described in further detail by Sobral et al. (2012). In summary, the overall contamination rate from non-HAEs in our sample is expected to be $\lesssim$10%.

The total number of galaxies detected in each field satisfying these selection criteria is 230 and 140 HAEs in COSMOS and UDS respectively. The higher number of HAEs in the COSMOS field is due to the difference in survey areas: HiZELS has so-far covered 1.23 deg$^2$ in COSMOS and 0.75 deg$^2$ in UDS. Note that the surface density of HAEs measured in the two independent fields is nearly identical, $\Sigma_{\mathrm{HAE}} \approx 190 \, \mathrm{deg}^{-2}$.

## 3 CLUSTERING ANALYSIS

### 3.1 Two-point angular correlation function estimator

We calculate the two-point angular correlation function, $\omega(\theta)$, using the estimator proposed by Landy & Szalay (1993),

$$\omega(\theta) = 1 + \left(\frac{N_R}{N_D}\right)^2 \frac{DD(\theta)}{RR(\theta)} - 2\frac{N_R}{N_D}\frac{DR(\theta)}{RR(\theta)}, \qquad (1)$$

where $N_D$ and $N_R$ are the number of galaxies in the data and random catalogue respectively, and $DD$, $RR$ and $DR$ are the number of data-data, random-random and data-random pairs at angular separation $\theta$. The modified Poissonian uncertainty is:

$$\delta\omega(\theta) = \frac{1 + \omega(\theta)}{\sqrt{DD(\theta)}}, \qquad (2)$$

although this certainly is an underestimate of the true error (we estimate the full covariance matrix in §3.2). For the random catalogue, we distribute $20N_D$ points uniformly over the survey areas, avoiding masked regions (cross-talk artifacts, bright stellar halos, etc.). We combine the results from the two independent survey volumes at the pair-counts stage, such that $DD = DD_{\mathrm{UDS}} + DD_{\mathrm{COSMOS}}$, etc. In practice this gives very similar results to averaging the individual $w(\theta)$, weighting by the Poisson uncertainty.

A correction must be applied to $w(\theta)$ due to the finite area surveyed and the fact that the mean density of galaxies is estimated from the sample itself and would be biased due to cosmic variance. The integral constraint ($C$; Groth & Peebles 1977) corresponds to a scale-independent underestimation of $\omega(\theta)$. As in Geach et al. (2008), we calculate $C$ following Roche et al. (1999):

$$C = \frac{\sum_i \omega(\theta_i)RR(\theta_i)}{\sum_i RR(\theta_i)}, \qquad (3)$$

where we model $\omega(\theta)$ using the scaled angular correlation function of dark matter, which is an excellent fit to the data and superior to a single power law (we discuss this analysis in §4.1). We evaluate equation 3 iteratively: first fitting the model to the data, calculating $C$ and then applying this correction to the data and fitting again, repeating this process until there is convergence. We find $C = 0.134$ for the combined area, and correct the measured $\omega(\theta)$ for this factor before fitting models.

### 3.2 Error estimation

We estimate the full covariance using the 'delete one jackknife' method (Shao 1986, and see Norberg et al. 2009 for a comprehen-

sive review of this and other error estimation methods). In short, the survey volume is split into $N$ sub-areas, and $\omega(\theta)$ calculated $N$ times, each time excluding one of the sub-areas. The elements of the covariance matrix are then given by:

$$\mathcal{C}_{ij} = \frac{N-1}{N}\sum_{k=1}^{N}(\omega_i^k - \bar{\omega_i})(\omega_j^k - \bar{\omega_j})' \qquad (4)$$

where $\omega_i^k$ is the correlation function (equation 1) measured for the $i$th angular bin, for the $k$th jackknife resampling, and

$$\bar{\omega_i} = \frac{1}{N}\sum_{k=1}^{N}\omega_i^k. \qquad (5)$$

We split the survey volume into 32 sub-regions and evaluate equation 1 for each jackknife realisation, omitting one sub-region each time. The uncertainty on the correlation function evaluated at each angular bin is given by $\delta\omega(\theta_i) = \sqrt{\mathcal{C}_{ii}}$ and this is used in the evaluation of $\chi^2$ difference between the data ($\omega$) and an arbitrary model ($\omega^{\mathrm{model}}$) taking into account covariance is

$$\chi^2 = (\omega - \omega^{\mathrm{model}})^{\mathrm{T}}\mathcal{C}^{-1}(\omega - \omega^{\mathrm{model}}), \qquad (6)$$

with the 1$\sigma$ uncertainty on a model parameter equivalent to the range $\Delta\chi^2 = 1$.

## 4 RESULTS

We present the results in Figure 1, corrected for the integral constraint, and including the covariance uncertainties evaluated in equation 4. Correlation functions are often fitted by a single power law, $\omega(\theta) = A\theta^{-\beta}$, usually with $\beta \approx 0.8$. This is adequate to fit the overall trend in the data, but the observed correlation function clearly deviates from a simple power law, especially at $\theta > 1'$. In part, the deviation of the observed correlation function at large separations is due to the break-down of Limber's approximation at $\theta \gtrsim 600''$ for samples where $\Delta z$ is narrow (Simon 2007, Sobral et al. 2010). In this case, even if the spatial correlation function is a power-law, the angular correlation function will depart from a power law at large angular separations. However, we also expect that a single power law is insufficient to model the clustering across the full angular range for physical reasons related to the relative clustering of satellite galaxies within single dark matter halos to the clustering of the halos themselves.

We explore this in the following sections, however for now we start our analysis with the simple power-law model fitted to data at scales $\theta \lesssim 600''$, which is useful for obtaining an estimate of the correlation length of the galaxies and easily comparable to the clustering of other populations. We perform minimised $\chi^2$ fits for the amplitude of the correlation function, fixing the slope with $\beta = 0.8$. We find a clustering amplitude $A = 29 \pm 4 \, \mathrm{arcsec}^{0.8}$, with a reduced $\chi^2/\nu = 0.9$. Throughout, we quote 1$\sigma$ uncertainties on the $\chi^2$ fit using the full covariance matrix calculated in equation 6.

If the real space correlation function can be assumed to be $\xi(r) = (r/r_0)^{-\gamma}$, where $r_0$ is the real-space correlation length and $\gamma = \beta + 1$, the amplitude of the correlation function $A$ can be related to $r_0$ using a version of Limber's equation (Limber 1954; Peebles 1980):

$$A = r_0^\gamma \frac{\Gamma((\gamma-1)/2)\Gamma(\gamma/2)}{\Gamma(1/2)}\int_0^\infty \frac{H_z}{c}\left(\frac{dn}{dz}\right)^2 \chi_z^{1-\gamma}dz, \qquad (7)$$
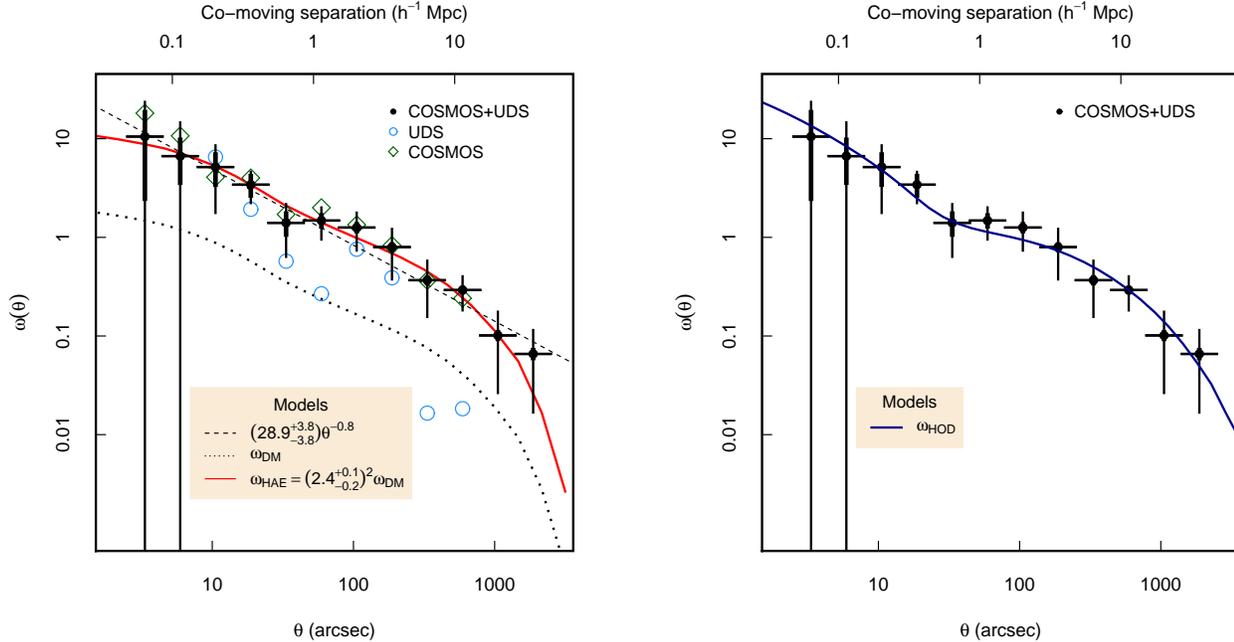
**Figure 1.** Two-point angular correlation function of HAEs in the COSMOS and UDS fields. (left) We show two model fits to the data: (a) a simple power law $A\theta^{-0.8}$ (dashed line) and (b) the projected correlation function of dark matter, scaled by a bias parameter, $b^2$ (dotted and solid lines). The power law is a reasonable fit to the general shape of the HAE correlation function, but the dark matter model also provides a good fit, and captures the deviation from a simple power law at all scales. The error bars are calculated from the diagonal elements of the covariance matrix which was estimated from the jackknife re-sampling method (we show for comparison the Poisson errors as thicker bars). The correlation function for the individual fields is also shown, however for clarity we do not show the error bars for these. Note that the combined COSMOS+UDS $\omega(\theta)$ values have been corrected for the integral constraint (§3.1, equation 3), whereas the individual fields have not. (right) Combined correlation function as (left), but shown with the best fitting HOD model (described in §4.3). The halo model successfully models the amplitude of the clustering strength on all measured scales, including the break at $\sim 1\,h^{-1}$ Mpc indicating the transition between the dominance of the one- and two-halo term in the halo model.

where $A$ is the amplitude of the correlation function evaluated at $\theta = 1$ radian, $\Gamma$ is the Gamma function, $H_z$ is the Hubble parameter at redshift $z$, $\chi_z$ is the co-moving radial distance to $z$ and $dn/dz$ is the redshift distribution of the population, normalised to unity. We assume the redshift distribution of HAEs in our narrowband selection is set by the $H_2S(1)$ filter profile, which can be described by a Gaussian function centred at $z = 2.233$, with full width at half maximum of $\delta z = 0.03$ (e.g. Sobral et al. 2010). Here we make the further assumption that we are 100% incomplete in the wings ($>$FWHM) of the $H_2S(1)$ transmission function, and therefore define the redshift distribution to be:

$$dn/dz = \begin{cases} n_0 \exp\left(-\frac{(z-z_c)^2}{2\sigma^2}\right) & \text{for } |z - z_c| < 0.015 \\ 0 & \text{for } |z - z_c| \geqslant 0.015, \end{cases} \quad (8)$$

where $z_c = 2.233$ and $\sigma = 0.0126$ and $n_0$ is the normalisation constant. This form of the redshift distribution attempts to account for the fact that there is a (luminosity dependent) bias in our selection in favour of HAEs with observed H$\alpha$ emission closer to the peak transmission of the filter. We are currently engaged in spectroscopic follow-up projects to properly characterise the redshift distribution of HAEs in our sample. Adopting this $dn/dz$ in equation 6, we find $r_0 = 3.7 \pm 0.3\,h^{-1}$ Mpc, which is similar to that derived in Geach et al. (2008) for a smaller sample. Note that the effect of applying a different redshift distribution on $r_0$ corresponds to a scaling in amplitude of $\int dz_a(dn_a/dz_a)^2/\int dz_b(dn_b/dz_b)^2$.

Contamination by non-HAEs reduces the amplitude of the correlation function by a factor $(1-f)^2$ where $f$ is the contamination fraction. As described in §2 it is likely that the contamination rate

is of order 10%, corresponding to a factor 0.8 attenuation in the clustering amplitude. We do not apply a correction to our measured parameters here until a more accurate estimate of the contamination rate is obtained from our spectroscopic survey.

### 4.1 Estimating the bias and characteristic halo mass of HAEs at z = 2.23

The autocorrelation function of galaxies can related to that of the underlying dark matter via the linear bias: $\xi_{DM} = b^2\xi_g$. This arises because galaxies forming in the peaks of a Gaussian random fluctuation field will be clustered in a way that is biased to that of the dark matter. This bias will depend on the details of galaxy formation relative to the underlying matter density. It is therefore an important part of our understanding of a particular galaxy population.

With an estimate for $\xi_{DM}$, we can fit the observed projected angular correlation function for the scaling $b^2$. To evaluate $\xi_{DM}$ (or rather, its projection, $\omega_{DM}$), we follow the method described by Hickox et al. (2012) and others (e.g. Myers et al. 2007; Coil et al. 2008) that we briefly review here. First, the projected angular correlation function of dark matter is derived by calculating the nonlinear dark matter power spectrum, $\Delta^2_{NL}(k, z)$, using the code HALOFIT (Smith et al. 2003), assuming $\Gamma = \Omega_m h = 0.21$ as the slope of the initial fluctuation power spectrum. The projected correlation function $\omega_{DM}(\theta)$, averaged over the redshift distribution of the HAEs, can then be calculated following Myers et al. (2007, equation A6), which projects the power spectrum into the angular

**Table 1.** Summary of model fit parameters to the observed clustering of HAEs at $z = 2.23$. Masses are in units of $h^{-1} M_\odot$ and uncertainties reflect $1\sigma$ range.

| Power-law[a] | |
|---|---|
| $r_0/(h^{-1}\,\mathrm{Mpc})$ | $\chi^2/\nu$ |
| $3.7 \pm 0.3$ | 0.9 |

| Dark matter[b] | | |
|---|---|---|
| $\log_{10}(M_{\rm h})$ | $b_{\rm HAE}$ | $\chi^2/\nu$ |
| $11.7 \pm 0.1$ | $2.4^{+0.1}_{-0.2}$ | 0.8 |

| Halo occupation distribution[c] | | | | | | |
|---|---|---|---|---|---|---|
| $\log_{10}(M_{\rm c})$ | $\log_{10}(M_{\rm eff})$ | $b_{\rm eff}$ | $f_{\rm sat}$ | $\sigma_{\log M}$ | $F_{\rm s}$ | $\chi^2/\nu$ |
| $12.6^{+0.5}_{-1.6}$ | $12.1^{+0.1}_{-0.2}$ | $2.4^{+0.3}_{-0.4}$ | $0.08^{+0.37}_{-0.04}$ | $0.62^{+0.64}_{-0.60}$ | $0.3^{+0.7}_{-0.2}$ | 0.7 |

[a] $\xi = (r/r_0)^{-1.8}$ fit for scales $\theta < 600''$.
[b] $\xi_{\rm gal} = b_{\rm gal}^2 \xi_{\rm DM}$. Mass is the 'characteristic' halo mass for the quoted bias.
[c] See section 4.3 for further details. Note: $\sigma_{\log M} = \delta_{\log M}$, $\alpha = 1$, $M_{\rm c} = M_{\rm min}$.

correlation function using Limber's equation. The dark matter correlation function is shown in Figure 1.

We fit for the $b^2$ scaling that minimises a $\chi^2$ fit with the observed HAE angular correlation function, yielding $b_{\rm HAE} = 2.4 \pm 0.1$, with reduced $\chi^2/\nu = 0.8$, formally slightly poorer than the power law fit. The characteristic halo mass $M$ is related to the bias through the parameterisation $b = f(\nu)$ where $\nu$ is the ratio of the critical threshold for spherical collapse to the r.m.s. density fluctuation for a mass $M$: $\nu = \delta_c/\sigma(M)$. The function $f(\nu)$ for a given cosmology is usually derived by fitting a form to the output of $N$-body simulations; here we apply the function of Tinker et al. (2010) (assuming halos are all 200 times the mean density of the Universe). The Tinker et al. fitting function is similar to that of Sheth, Mo & Tormen (2001), but predicts slightly larger $b$ for large $\nu$ and slightly lower $b$ for small $\nu$ (asymptoting to constant $b$ for low mass halos, and scaling as a power law for high masses). For a bias of $b_{\rm HAE} = 2.4^{+0.1}_{-0.2}$, we calculate a characteristic halo mass of $\log_{10}(M_{\rm h}/[h^{-1} M_\odot]) = 11.7 \pm 0.1$ at $z = 2.23$. This characteristic $M_{\rm halo}$ corresponds to the top-hat virial mass (see e.g. Peebles 1993 and references therein), in the simplified case in which all objects in a given sample reside in halos of the same mass. We note that this mass is approximately equal to the 'effective' halo mass derived from full HOD modelling, as discussed in §4.3, but differs from some prescriptions in the literature which assume that sources occupy all halos above some minimum mass. Given the halo mass function at $z \sim 2$ (e.g. Tinker et al. 2008) the derived minimum mass is typically a factor of $\sim 2$ lower, for the same clustering amplitude, than the characteristic mass quoted here.

**4.2 Comparison to models of galaxy formation**

GALFORM (Cole et al. 2000) is a successful semi-analytic model, or rather a suite of models, that describe galaxy formation using simplified prescriptions for the radiative cooling of gas within dark matter halos, star formation and feedback (both through supernovae and active galactic nuclei [AGN]), along with a hierarchical component for growth set by the merger histories of the halos the galaxies occupy. The latter is achieved by coupling semi-analytic models to large $N$-body simulations in which halos (usually defined as regions within which the matter density is $\Delta = 200 \times \bar{\rho}(z)$) can be identified and tracked (see Merson et al. 2012 in preparation).

The main criticism levelled at semi-analytics is that they are over-complicated with too many free (and uncertain) parameters. The counter argument is that galaxy formation is inherently complex, and semi-analytics serve as a tool for exploring the physics shaping the evolution of the galaxy population below the resolution that can be achieved in numerical simulations; these models can be refined as empirical results improve. Furthermore, semi-analytic models are successful in reproducing many of the key features of the galaxy population, including the shape and evolution of the luminosity functions of stellar mass (see Baugh 2006 for a review).

We consider the clustering properties of HAEs within the Millennium Simulation (Springel et al. 2005), generated from three different GALFORM simulations: Bower et al. (2006; B06), Font et al. (2008; F08) and Lagos et al. (2011; L11). The B06 model, which includes a recipe for AGN-driven feedback in massive halos, successfully reproduces key features of the local and distant galaxy population, including the black hole–bulge mass scaling at $z = 0$, the shape of the $b_{\rm J}$- and $K$-band luminosity functions at $z = 0$ (successfully reproducing the exponential turn down at high luminosities) and the evolution of the stellar mass function of galaxies out to $z \sim 4.5$. Orsi et al. (2010) studied the clustering of HAEs in the B06 model to assess the relative merits of different selection techniques for the construction of future galaxy redshift surveys. The F08 and L11 models are based on B06, with the key improvements that: (a) F08 includes a more realistic prescription for gas cooling within satellite galaxies which orbit within massive halos, and (b) L11 implements a pressure-based star formation law following Blitz & Rosolowsky (2006), and a more refined model of the ISM. We refer the reader to the respective articles that describe each model in detail. The selection of HAEs in GALFORM is described by Orsi et al. (2010).

The predicted galaxy correlation functions are effectively identical in slope and amplitude in all three models, with $r = 3.8$–$4.2\,h^{-1}$ Mpc when the amplitude of the real space correlation function is equal to unity $\xi(r) = 1$. The similarity between the predictions is perhaps not surprising, given the similarities in the underlying galaxy formation models. This is in reasonable agreement with the amplitude of the real space correlation function estimated from the de-projection of the angular correlation function of real HAEs. In Figure 2 we compare $\xi(r)$ measured directly from the simulations to our power law and scaled dark matter models of the real HAE angular correlation function. As Figure 2 shows, both power law and scaled dark matter fits to the data almost ex-
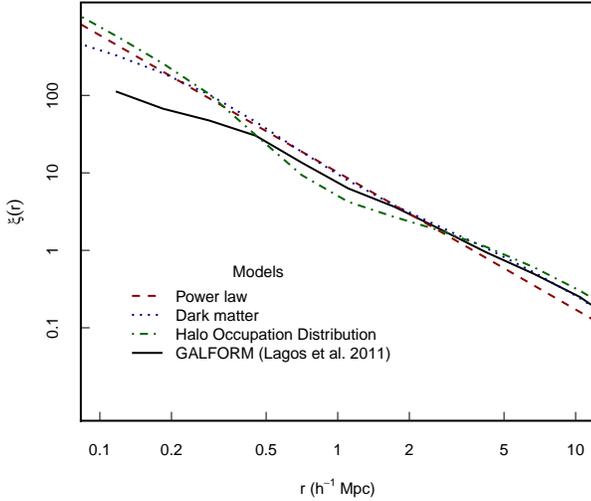
**Figure 2.** A comparison of the real space correlation function of simulated HAEs from GALFORM with $L_{H\alpha} > 10^{42} \, \text{erg s}^{-1} \, \text{cm}^{-2}$ at $z = 2.2$ to fits of the observed angular clustering (Fig 1). The lines show three model fits to the measured angular correlation function: (a) a simple power law $\xi(r) = (r/r_0)^{-\gamma}$ (with $\gamma = 1.8$), (b) $\xi(r) = b^2 \xi_{DM}$ and (c) the HOD fit (see §4.3). On scales $\gtrsim 0.5$ Mpc the models predict HAE clustering that is in reasonable agreement with the amplitude of the clustering measured in the observations, but the semi-analytic models predict less power at low separation compared to the data (this is also apparent in the Bower et al. and Font et al. models which we do not show here for clarity).

actly match the clustering strength of GALFORM HAEs on scales $r > 0.5 \, h^{-1}$ Mpc. GALFORM has less clustering than scaled dark matter at smaller (single halo) scales. We explore this in the next section, with a more sophisticated model of the clustering of HAEs than simple using a scaled version of the dark matter correlation function.

## 4.3 A Halo Occupation Distribution model for HAEs at z = 2.23

### 4.3.1 Overview

A basic tenet of our current picture of the formation of galaxies, and their relationship to dark matter, is that galaxies inhabit dark matter halos either as 'central' galaxies close to the density peak, or 'satellites' distributed according to some radial density profile (Navarro, Frenk & White 1997). Intuitively, the number of satellites a halo can accommodate increases with halo mass; illustrated in the real Universe by massive clusters of galaxies, where the central galaxy is usually a massive elliptical surrounded by hundreds or thousands of lower-mass cluster members. However, although the occupation number might scale with halo mass in the stellar mass limited case, the exact selection of galaxies in a given sample will affect the observed halo occupation distribution. A halo occupation distribution (HOD) model parameterises the probability distribution that describes the likelihood that a halo of mass $M$ hosts on average $N$ galaxies (see Cooray & Sheth 2002 for a review). As the projected clustering and number density of a galaxy population (or populations) will depend on the form of the HOD, we can use the observed clustering data to try to constrain models of the halo occupation of HAEs. Critical to this approach is the parame-

terisation of the HOD; namely the functional form assumed for the probability of finding a central galaxy, or $N$ satellites in a halo of mass $M$.

We follow the methods of Wake et al. (2008, 2011 [W11]) to construct a halo model, and refer the reader to Appendix B of W11 for a thorough description. In brief, one must parameterise the halo model by defining functions for the mean number of galaxies in a given halo, $\langle N|M \rangle$. Given the good agreement between the clustering amplitude measured from the semi-analytic models and the data, we adjust our fiducial halo model to match the simulations; here we have the luxury of the direct prediction of the HOD from the model. In Figure 3 we show the HOD of $1.45 \times 10^7$ dark matter halos in the Millennium Simulation, populated with HAEs using the GALFORM model. We show the HAE HOD for three luminosity cuts, $L_{H\alpha} > 10^{41}, 10^{42}, 10^{43} \, \text{erg s}^{-1}$.

The star-forming galaxy HOD has some important differences from typical mass limited HODs (cf. Zheng et al. 2007, W11) that are worth noting. First, at the lowest halo masses, the central galaxy distribution is approximately Gaussian, with a characteristic host mass $M_{min}$ and scale $\sigma$. At halo masses $M \gtrsim M_{min} + \sigma$ the distribution of centrals becomes approximately flat, similar to the mass limited case though does not necessarily asymptote to $\langle N_c|M \rangle = 1$. One could therefore envisage a simple two component model for the central HAE halo occupation, with a Gaussian distribution plus step function. At low H$\alpha$ luminosities, $L_{H\alpha} \sim 10^{41} \, \text{erg s}^{-1}$, above halo masses of $\sim 10^{11} h^{-1} \, M_\odot$ almost every halo hosts a central that is a HAE. As the luminosity limit is increased, the low-mass Gaussian component becomes more prominent (peaked) and shifted to higher halo masses, but with the occupation number declining with increasing H$\alpha$ at all halo masses.

The decline in occupation number within increasing H$\alpha$ luminosity is in part due to the form of the luminosity function, but the shape of the central HOD is likely to be driven by (a) the stellar mass and star formation history of central galaxies as a function of halo mass and (b) differences in the star formation efficiency as a function of halo mass (e.g. the cooling rate onto central galaxies). It is also important to consider that H$\alpha$ emission can also result from nuclear activity which might be important for bright, central HAEs in massive halos. The satellite distribution is similar to the mass-limited case, with a smooth lower-mass cut-off in occupation and $\langle N_s|M \rangle$ scaling as a power-law at large $M$ (Kravtsov et al. 2004; Zheng et al. 2005). There is a simple luminosity dependence, with the number of satellites declining as $L_{H\alpha}$ increases. The decline in satellite occupation at all mass scales for the more luminous HAEs is a natural outcome of the shape of the luminosity function, with $L_{H\alpha} = 10^{43} \, \text{erg s}^{-1}$ probing exponentially declining $L > L^\star$ HAEs at this redshift (Geach et al. 2008; Sobral et al. 2012).

### 4.3.2 A HOD model for H$\alpha$ emitters

The central HAE distribution can be adequately described by two components:

$$\langle N_c|M \rangle = F_c^B (1 - F_c^A) \exp\left[-\frac{\log(M/M_c)^2}{2\sigma_{\log M}^2}\right]$$
$$+ F_c^A \left[1 + \text{erf}\left(\frac{\log(M/M_c)}{\sigma_{\log M}}\right)\right] \quad (9)$$

where $F_c^{A,B}$ are normalisation factors ranging from 0–1. The first component describes the Gaussian distribution of centrals around
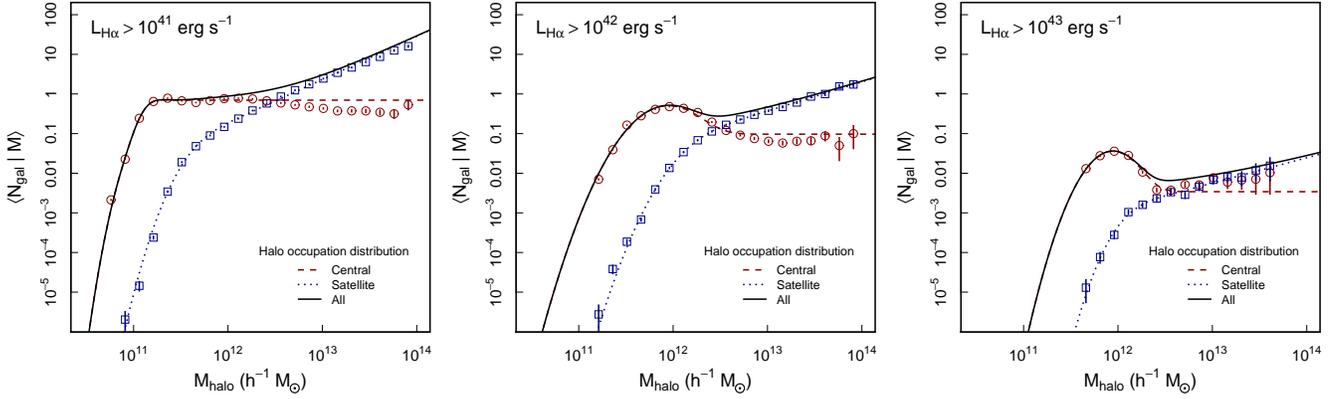
**Figure 3.** Halo occupation distribution (HOD) model of HAEs at $z = 2.2$ predicted by GALFORM, where $\langle N_{\mathrm{gal}}|M \rangle$ denotes the mean number of galaxies in a halo of mass $M$. We show the HODs of central and satellite galaxies with H$\alpha$ luminosities of (left to right panels) $L_{\mathrm{H}\alpha} > 10^{41}$, $10^{42}$, $10^{43}$ erg s$^{-1}$ (points). The total number of halos (that occupy the Millennium Simulation volume) in this model is $1.45 \times 10^7$ (error bars are Poisson). There is a clear luminosity dependence to the HOD, with the occupation number dropping at all halo masses with increasing H$\alpha$ luminosity. The lines corresponding to 'central', 'satellite' and 'total' show the best fit to the points extracted from GALFORM using our parametric HOD described in §4.3. At all luminosities we can fit the HOD with same parametric form, and we adopt this model in our fitting of the observed projected correlation function.

halos of average mass $M_c$, and the second component describes the high mass distribution, which we take as the standard mass-limited step function form (Zheng et al. 2007). The parameter $\sigma_{\log M}$ describes the typical mass range of halos with HAEs as centrals for the Gaussian component; the exact value of $\sigma_{\log M}$ in the second component is not critical, and so we decide to fix it to the Gaussian width. Similarly we set the step function low mass cut-off to be $M_c$. As shown in Figure 3, this four parameter model provides a good description of the model HOD at $10^{41} < (L_{\mathrm{H}\alpha}/\mathrm{erg\,s}^{-1}) < 10^{43}$, the pertinent range for our analysis.

The number of satellite galaxies is described by a smoothed step function similar to the central galaxy distribution for mass limited samples (Zheng et al. 2007), but with the added component of a power law scaling at masses larger than the critical mass, $M_{\min}$:

$$\langle N_{\mathrm{s}}|M \rangle = F_{\mathrm{s}}\left[1 + \mathrm{erf}\left(\frac{\log(M/M_{\min})}{\delta_{\log M}}\right)\right]\left(\frac{M}{M_{\min}}\right)^{\alpha}. \quad (10)$$

The parameter $F_{\mathrm{s}}$ is the mean number of galaxies at the transition mass $M_{\min}$ (the characteristic mass above which halos can contain satellite HAEs). The parameter $\alpha$ controls the abundance of star-forming satellites for $M > M_{\min}$. This functional form provides a more satisfactory fit to the model satellite distribution at low masses allowing a more gradual cut off to the power law than is assumed in the standard stellar mass limited case (e.g. Wake et al. 2011). We make no restrictions as to whether a central HAE is required for the hosting of satellites, so the mean total number of galaxies in a halo of mass $M$ is

$$\langle N|M \rangle = \langle N_{\mathrm{c}}|M \rangle + \langle N_{\mathrm{s}}|M \rangle. \quad (11)$$

There are up to eight free parameters in this HOD. However we choose to fix some in our modelling, given the size of the current sample. The exact smoothing of the satellite low mass cut-off is not particularly important, in that satellites close to the threshold (in the model) do not contribute significantly to the halo occupation. Therefore we fix $\delta_{\log M} = \sigma_{\log M}$. Although we do not require a halo to contain a H$\alpha$ emitting central in order to host satellite HAEs, we also constrain the satellite threshold mass as $M_{\min} =$

$M_c$. Finally, we fix the slope of the satellite distribution to $\alpha = 1$; this is close to the model fit across the full luminosity range shown in Figure 3, and is in agreement with the value found for mass limited samples. Thus, our model has five free parameters. Note that having a consistent model that scales with H$\alpha$ luminosity is of benefit to our analysis, given the possible uncertainties in the fidelity of observed and simulated H$\alpha$ fluxes.

With $\langle N|M \rangle$ defined, the number density of galaxies is given by the integral of the halo mass function $n(M)$:

$$n_g = \int dM n(M) \langle N|M \rangle, \quad (12)$$

and this can be used as an additional constraint in the fitting of the HOD, provided the number density of galaxies is known, although it is often difficult to produce fits that simultaneously match the clustering and abundance, e.g. Quadri et al. (2008). Here we use the latest parameterisation for $n(M)$ from Tinker et al. (2010). With the halo model set up, $\xi(r)$ is defined (Cooray & Sheth 2002), and this can be projected to the angular correlation function $\omega(\theta)$ using Limber's equation.

We can also define other parameters that are useful to summarize the halo model: the satellite fraction,

$$f_{\mathrm{sat}} = \int dM n(M) \langle N_{\mathrm{c}}|M \rangle \langle N_{\mathrm{s}}|M \rangle / n_g, \quad (13)$$

which measures the fraction of galaxies in the sample that are satellites; the effective halo mass:

$$M_{\mathrm{eff}} = \int dM M n(M) \langle N|M \rangle / n_g, \quad (14)$$

and the effective galaxy bias

$$b_g = \int dM n(M) b(M) \langle N|M \rangle / n_g, \quad (15)$$

where $b(M)$ is the bias for a halo of mass $M$.

*4.3.3   HOD fitting results*

We assert from the outset that, with the current data (i.e. relatively small sample number), the interpretation of the results of this HOD analysis must be taken with caution. Given the degeneracies involved, the results should only be used as an early guide. Nevertheless, the HOD provides an elegant framework within which to discuss the observed clustering, and we examine the results here.

The angular correlation function derived from the HOD described above is fit to the data, including the full covariance matrix. As in W11, minimisation is achieved by using a Markov Chain Monte Carlo technique, which allows us to efficiently explore the parameter volume. The best fit $\omega(\theta)$ is shown in Figure 1, with a reduced $\chi^2/\nu = 0.7$, again indicating that our data is too coarse to constrain the model. Although we present the best fitting model here, there are large degeneracies in the current halo model that the data cannot resolve. This means that the key halo parameters described in §4.3.2 are only poorly constrained. The difference between the HOD model and the real space correlation function measured from GALFORM simulations is shown in Figure 2. Most of the parameters in equations 9 and 10 have very poor constraints, For example, the normalisation factors are effectively unconstrained, and the 68% confidence interval for the minimum halo mass hosting centrals (and the minimum mass for satellites) is large, $M_c \sim (0.1-13) \times 10^{12} h^{-1} M_\odot$ and the $1\sigma$ upper limit of the satellite fraction $f_{\rm sat} \lesssim 0.46$. The normalisation factors $F_c^{A,B}$ are effectively unconstrained.

There are clearly indications of serious degeneracies in the model that cannot be resolved with the current data and are a common problem for samples of galaxies where just a small fraction of the population are detected. Only the average bias and mean halo mass are reasonably well constrained, with $b = 2.4^{+0.3}_{-0.4}$ and $M_{\rm eff} = (1.3^{+0.4}_{-0.5}) \times 10^{12} h^{-1} M_\odot$, in agreement with what was found for the scaled dark matter fit in §4.1. We summarise the results from the HOD fit in Table 1, along with the results from the power-law and dark matter fits.

## 5   DISCUSSION

### 5.1   The fate of HAEs at z = 2.23

The clustering amplitude of $z = 2.23$ HAEs is similar to other star-forming populations at high-$z$. Adelberger et al. (2005) present a clustering analysis of $U_nG\mathcal{R}$ (BX/BM) selected star-forming galaxies at $1.4 < z < 3.5$ and derive a correlation length of $r_0 \sim 4h^{-1}$ Mpc across this redshift range, and argue that, at $z \sim 2.2$, star-forming (BX) galaxies with $M_\star \approx 10^{10} M_\odot$ reside in dark matter halos of mass $\sim 10^{12} M_\odot$. Hayashi et al. (2007) present a clustering analysis of star-forming 'sBzK' selected galaxies (Daddi et al. 2004) at $z \sim 2$, which are a similar population to the broad-band BX selected galaxies described above, finding $r_0 = 3.2^{+0.6}_{-0.7} h^{-1}$ Mpc and typical halo masses of $2.8 \times 10^{11} M_\odot$.

The average stellar mass of HAEs in our sample is $\log(M_\star/M_\odot) = 9.4$ (calculated from stellar population fits to the homogenised UV-optical-near-IR photometry using the templates of Bruzual & Charlot 2007, including the thermally pulsating Asymptotic Giant Branch population, Sobral et al. 2011). The key improvement made here is that our selection is far more exclusive than broad band selections, with the narrowband technique corresponding to a nearly pure SFR selection over a very narrow redshift range. This has the effect of minimising contamination (important for an accurate measurement of the clustering amplitude for a spe-
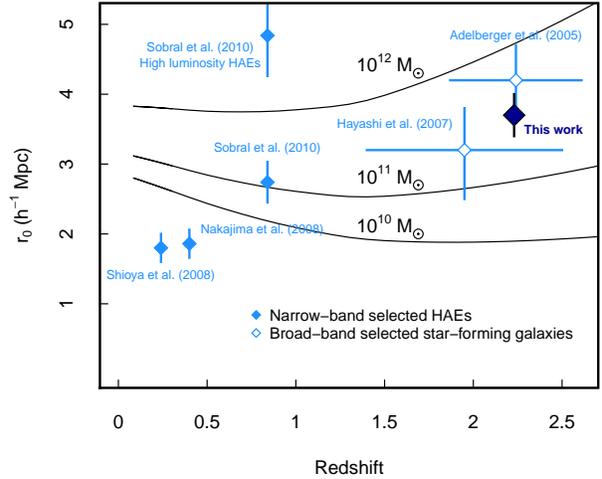


**Figure 4.** Comparison of the correlation length of HAEs and star-forming galaxies since $z = 2.2$ derived from de-projected angular clustering measurements. We compare the measured values to the predicted halo mass hosting galaxies with correlation length $r_0$ for our cosmology. We distinguish between measurements made from samples of HAEs selected in narrow-band and more general star-forming galaxies selected in broad-band surveys (the latter have much broader redshift distributions). Note that evolutionary trends are hard to measure in this plot, given that the low redshift surveys generally probe lower luminosity systems, and there is observed to be a strong correlation between clustering strength and luminosity (i.e. SFR). Indeed, Sobral et al. (2010) show that $r_0$ increases to $r_0 \sim 5h^{-1}$ Mpc at $z = 0.84$ when $L_{\rm H\alpha} \gtrsim 10^{42}$ erg s$^{-1}$ are considered. In summary, 'normal' star-forming galaxies with SFR $\sim 1-100 M_\odot$ yr$^{-1}$ have been hosted by dark matter halos with $10^{10} \lesssim M_{\rm h} \lesssim 10^{12} h^{-1} M_\odot$ since $z = 2.2$, with more luminous and massive systems residing in more massive halos at all epochs.

cific population) and the tomographic nature of the selection should improve the contrast of scale dependent features in the projected clustering.

Hayashi et al. note the clear stellar mass ($K$-band luminosity) dependence to the clustering strength, indicating that the descendants of sBzK galaxies could range from sub-Milky Way mass halos to halos similar to rich clusters. Sobral et al. (2010) also find that, when split by stellar mass and H$\alpha$ luminosity, a clear increase in the derived correlation length was found for HAEs at $z = 0.84$, such that more massive and luminous (i.e. high SFR) galaxies reside in more massive dark matter halos. The 'varied fates' of star-forming galaxies at $z = 2$ has been discussed by Conroy et al. (2008) who examine the evolutionary history of star-forming galaxy hosting dark matter halos in $N$-body simulations, finding that generically selected star-forming galaxies at $z \sim 2$ do not evolve into any single class of galaxy by $z = 0$. The number density of the descendants of model $z \sim 2$ star-forming galaxies at $z = 0$ drops by a factor of two due to the merging of descendants in the interval $0 < z < 2$. Of the remaining galaxies that did not merge, 70% evolve into central galaxies within halos of $M_{\rm h} \gtrsim 10^{12} h^{-1} M_\odot$ by $z = 0$. Central galaxies at $z = 0$ correspond to $\gtrsim L^\star$ systems, whereas the star-forming galaxies that are destined to become satellites by $z = 0$ are generally lower-mass systems owing to the slower/halted rate of stellar mass growth expected for sub-halos orbiting within massive halos (i.e. a decline in the cooling rate and potential expulsion of gas, q.v. §4.2). González

et al. (2011) find a similar result for submillimeter selected galaxies within GALFORM, with the descendants of these high-$z$ star-forming galaxies evolving into $z = 0$ galaxies with stellar masses $M_\star \sim 10^{10-12}h^{-1}M_\odot$.

Although we expect the HAEs in our sample to evolve into a range of galaxy types, we can estimate the halo mass of the descendants of the average HAE in our sample – i.e. those hosted by halos with the 'characteristic' mass found in our clustering analysis. Assuming $M_{\rm eff} = (1.3^{+0.4}_{-0.5}) \times 10^{12}h^{-1}\,M_\odot$ at $z = 2.23$ we use the median halo mass growth rate from Fakhouri, Ma & Boylan-Kolchin (2010) to estimate that by $z = 0$ the average HAE is destined to reside in a halo of mass $M_{\rm h} = 2$–$5 \times 10^{12}h^{-1}M_\odot$. Thus, HAEs are an important population to study in the context of understanding the ecology of 'typical' galaxies in the local Universe, although as described above, there are likely to be important mass and luminosity dependencies in the exact evolutionary trajectory of HAEs (as hinted at by Figure 3 and 4), which our current data cannot resolve.

## 5.2 Comparison with other Hα surveys at low redshift

Sobral et al. (2010) present a clustering analysis of HAEs detected in HiZELS at a redshift of $z = 0.84$ (narrow $J$-band selection, probing to lower Hα luminosities than the present survey) and find a strong luminosity dependence to the clustering strength, $2 \lesssim r_0 \lesssim 5h^{-1}\,$Mpc for $41.6 < \log(L_{\rm H\alpha}/{\rm erg\,s}^{-1}) < 43.2$, with the clustering strength increasing with luminosity (similar to the trend seen in other samples, as described above). Our sample is too small to split into luminosity bins and retain sufficient signal-to-noise in the clustering measurement. At an equivalent luminosity limit to the one used in our analysis, the clustering strength of HAEs at $z = 0.84$ is similar to that at $z = 2.23$, indicating only weak evolution in the clustering properties of star-forming galaxies with SFR$\gtrsim$10 $M_\odot$ yr$^{-1}$ over this range. Shioya et al. (2008) and Nakajima et al. (2008) present clustering analyses for HAEs at $z = 0.24$ and $z = 0.4$ respectively, finding correlation lengths of $\sim$1.5–2 $h^{-1}$ Mpc. However, those studies probe fainter HAEs than our sample contains, and therefore it is difficult to assess any redshift evolution in the clustering properties of HAEs to these later epochs given the expected strong luminosity dependence of $r_0$.

We summarise this comparison in Figure 4, where we compare the derived correlation length of samples of narrow-band selected HAEs and the more generic broad-band selections of star-forming galaxies described above. The broad range in luminosity limits (Shioya et al. 2008 probe Hα luminosities over two orders of magnitude lower than our sample) in the $r_0$–$z$ plot mask any evidence of evolution in the clustering of star-forming galaxies. Indeed, the characteristic luminosity of HAEs is itself a strong function of redshift, with $\log(L^\star/{\rm erg\,s}^{-1}) = 0.45z + 41.87$ since $z = 2.23$ (Sobral et al. 2012). It is clear however, that 'typical' star-forming galaxies (i.e. those close to $L^\star$ and not in the ultraluminous class, such as submillimeter selected galaxies, see Hickox et al. 2012) have, on average, been hosted by dark matter halos with $10^{10} \lesssim M_{\rm h} \lesssim 10^{12}\,h^{-1}\,M_\odot$ since $z = 2.2$, with the amplitude of clustering decreasing for less luminous and lower mass systems.

Figure 4 presents an average representation of the clustering properties of star-forming galaxies. In reality, HAEs are expected to reside in halos with a range of masses (as modelled by our HOD for example), and this will have important consequences for their fate. In the next section we illustrate this with an example from our data – an apparent over-density of HAEs in the COSMOS field,
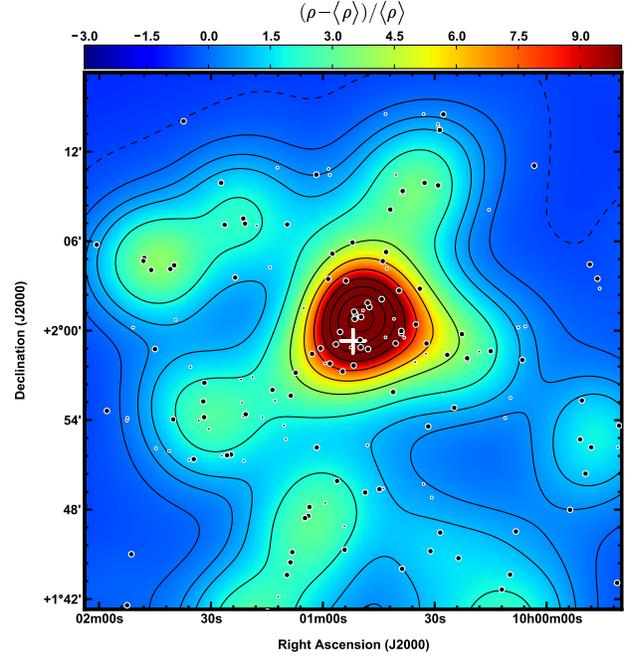
**Figure 5.** A potentially massive halo in the COSMOS field, blindly detected as an over-density of HAEs in HiZELS. The large points show HAEs meeting the selection criteria used in the present study (smaller points are HAEs with lower line fluxes). The colour background and contours show the smoothed density contrast, $\delta = (\rho - \langle\rho\rangle)/\langle\rho\rangle$, clearly indicating a significant peak in the mean surface density. Interestingly, this structure contains a Hα emitting $z = 2.23$ QSO close to the peak (cross symbol); such active systems are often used as 'signpost' objects around which to search for over-dense structures. HAEs in this structure exemplify contribution of star-forming satellites producing power in the correlation function at low angular separations.

perhaps representing star-forming galaxies tracing a rather massive, rare dark matter halo.

## 5.3 A comment on satellite HAEs and cosmic variance: the detection of a over-dense structure in the COSMOS field

The measured correlation function implies that satellites play a non-negligible role in the small-scale clustering power. In the halo model described in §4.3, massive halos with large numbers of bright Hα–emitting satellites are rare objects, as dictated by the luminosity and halo mass function. However such systems might be detectable in large surveys such as ours as local over-densities in the surface density of HAEs. We have detected such a system in the COSMOS field.

We have evaluated the local density contrast across the field by first calculating a simple local density measure $\rho = 4/\pi r_4^2$, where $r_4$ is the angular distance to the fourth nearest HAE from an arbitrary point. This is normalised to give the density contrast: $\delta = (\rho - \langle\rho\rangle)/\langle\rho\rangle$, where $\langle\rho\rangle$ is the mean surface density of HAEs across the field. We evaluate $\delta$ across a grid, and then smooth this with a Gaussian kernel of FWHM equivalent to 5 co-moving Mpc. The peak density contrast is $\delta = 17$ at $10^{\rm h}00^{\rm m}50^{\rm s}$, $+02°00'53''$. We do not detect a similar structure in the UDS field, implying the sky density of environments of similar mass is of the order one per two square degrees. Systems such as this illustrate the importance of taking into account cosmic variance in clustering mea-

surements of HAEs. As Figure 1 shows, the small-scale clustering power in the angular correlation function is dominated by the COSMOS field, and this local over-density is likely to be a dominant contributing factor, with the one-halo term boosting $\omega(\theta)$ at scales below 1 Mpc. The cosmic variance uncertainty is encoded into the delete-one jackknife method we have employed, since the bulk of the over-density is easily encompassed by one of the sub-volumes.

Figure 5 shows the sky plot of HAEs around the peak of the over-density, including a representation of the smoothed density field. Interestingly, the peak encompasses the $z = 2.2396$ quasar SDSS J100051.92+015919.2 (Prescott et al. 2006), which is itself a HAE (and included in our sample). Extremely luminous galaxies such as quasars and radio galaxies are often used to seek out dense environments, relying on the fact that these extreme, but rare, active galaxies are likely to be highly biased tracers of the matter field and therefore reside in massive halos (Ellingson et al. 1991; Clowes & Campusano 1991; Bower & Smail 1997; Miller et al. 2004; Boris et al. 2007; Hatch et al. 2011; Matsuda et al. 2011). In this case the COSMOS structure was blindly detected and turns out to harbour a quasar, lending support for the approach of imaging the fields of active galaxies with narrowband surveys to discover such (rare) environments.

## 6  SUMMARY

We have presented an analysis of the clustering properties of 370 H$\alpha$ emitting galaxies at $z = 2.23$, selected in two, independent, degree-scale fields as part of the HiZELS survey. Using a series of increasingly sophisticated models of the clustering, we find:

(i) The average correlation function can be broadly modelled as a power law, with slope $\beta = 0.8$. Although there are clear deviations from the simple power law on all scales, the normalisation of the power law fit provides an adequate estimate of the physical correlation length of HAEs $r_0 = 3.7 \pm 0.3\,h^{-1}$ Mpc, similar to other star-forming populations at this redshift. We find that the latest semi-analytic models of galaxy formation predict a correlation length that is in good agreement with the measured value.

(ii) The shape of the observed correlation function is more accurately reproduced by scaling the projected correlation function of dark matter with a bias factor: $\omega_{\mathrm{HAE}} = b^2 \omega_{\mathrm{DM}}$. This is superior to the simple power law as it is a better description of the variation of the power in the correlation function across the full range of measured scales, $0.1 < r < 10\,h^{-1}$ Mpc. The best fitting value HAEs is $b_{\mathrm{HAE}} = 2.4^{+0.1}_{-0.2}$. This can be related to a characteristic halo mass, which we find to be $\log(M_{\mathrm{h}}/[h^{-1}M_\odot]) = 11.7 \pm 0.1$.

(iii) Our final model attempts to fit the HAE clustering using a halo occupation distribution (HOD) model. To parameterise the occupation of central and satellite HAEs in dark matter halos, we turn to the semi-analytic models for motivation (which predict the HOD), given the good agreement between model described above. Although the HOD is poorly constrained by the current data (with clear degeneracies resulting in multiple acceptable fits to the angular clustering), we derive an average bias and characteristic halo mass in good agreement with those derived from the scaled dark matter correlation function, with $b = 2.4^{+0.3}_{-0.4}$ and effective halo mass $M_{\mathrm{eff}} = (1.3^{+0.4}_{-0.5}) \times 10^{12} h^{-1}\,M_\odot$.

(iv) Finally, we report on the detection of a significant localised over-density of HAEs in the COSMOS field. Interestingly, this structure encompasses a $z = 2.23$ QSO, which is itself a HAE. It is clear from the clustering analysis that cosmic variance in HAE

surveys remains important on $\sim 1\,\mathrm{deg}^2$ scales, especially in the fluctuations expected in the small scale clustering amplitude. The HAE structure is likely to trace a relatively massive halo, $M_{\mathrm{h}} \sim 10^{13}\,M_\odot$ with a high satellite occupation number, and could be destined to evolve into a large group or cluster of galaxies by $z = 0$.

Future high redshift H$\alpha$ surveys with improved statistics over wider fields will be able to explore halo models of HAEs in further detail. Our current result represents a first step in this direction, and despite the limited information we can extract from the clustering models, it is clear that disentangling the relative role of central and satellite star formation in massive halos at high redshift is an important component of our understanding of the efficiency of stellar mass assembly as a function of halo mass. Multi-epoch H$\alpha$ surveys such as HiZELS will be essential for examining evolutionary trends in the clustering properties of star-forming galaxies at the peak era of galaxy formation, and we aim to investigate this in a forthcoming paper.

## REFERENCES

Adelberger, K. L., Steidel, C. C., Pettini, M., Shapley, A. E., Reddy, N. A., Erb, D. K, 2005, ApJ, 619, 697

Baugh, C. M., 2006, A primer on hierarchical galaxy formation: the semi-analytical approach, Reports on Progress in Physics, 69, 3101–3156

Benson, A. J., Cole, S., Frenk, C. S., Baugh, C. M., Lacey, C. G., 2000, MNRAS, 311, 793

Best, P., Smail, I., Sobral, D., Geach, J., Garn, T., Ivison, R., Kurk, J., Dalton, G., Cirasuolo, M., Casali, M., 2010arXiv1003.5183

Blakeslee et al. 2003, ApJ, 596, L143

Blitz, L., Rosolowsky, E., 2006, ApJ, 650, 933

Boris, N. V., Sodré, L., Jr., Cypriano, E. S., Santos, W. A., de Oliveira, C. Mendes, West, M., 2007, ApJ, 666, 747

Bower, R. G., Smail, Ian, 1997, MNRAS, 290, 292

Bower, R. G., Benson, A. J., Malbon, R., Helly, J. C., Frenk, C. S., Baugh, C. M., Cole, S., Lacey, C. G., 2006, MNRAS, 370, 645

Bruzual, G., 2007, From Stars to Galaxies: Building the Pieces to Build Up the Universe. ASP Conference Series, Vol. 374, Edited by Antonella Vallenari, Rosaria Tantalo, Laura Portinari, and Alessia Moretti., p.303

Clowes & Campusano 1991, MNRAS, 249, 218

Cole, S., Lacey, C. G., Baugh, C. M., Frenk, C. S., 2000, MNRAS, 319, 168

Colless, M, et al., 2001, MNRAS, 328, 1039

Coil, A. L., et al. 2008, ApJ, 672, 153

Conroy, C., Shapley, A. E., Tinker, J. L., Santos, M. R., Lemson, G., 2008, ApJ, 679, 1192

Cooray, A., Sheth, R., 2002, PhR, 372, 1

Daddi, E., Cimatti, A., Renzini, A., Fontana, A., Mignoli, M., Pozzetti, L., Tozzi, P., Zamorani, G., 2004, ApJ, 617, 746

Elbaz, D., et al., 2011, A&A, 533, 119

Ellingson, E., Yee, H. K. C.; Green, R. F., 1991, ApJS, 76, 455

Fakhouri O., Ma C.-P., Boylan-Kolchin M., 2010, MNRAS, 406, 2267

Font, A. S., Bower, R. G., McCarthy, I. G., Benson, A. J., Frenk, C. S., Helly, J. C., Lacey, C. G., Baugh, C. M., Cole, S., 2008, MNRAS, 389, 1619

Geach, J. E., Smail, Ian, Best, P. N., Kurk, J., Casali, M., Ivison, R. J., Coppin, K., 2008, MNRAS, 388, 1473

González, J. E., Lacey, C. G., Baugh, C. M., Frenk, C. S., 2011, MNRAS, 413, 749

Groth, E. J., Peebles, P. J. E., 1977, ApJ, 217, 385

Guaita, L., et al., 2010, ApJ, 714, 255

Hall & Green 1998, 507, 558

Hatch, N. A., et al. 2011, MNRAS, 410, 1537

Hayashi, M., Shimasaku, K., Motohara, K., Yoshida, M., Okamura, S., Kashikawa, N., 2007, ApJ, 660, 72

Hickox, R. C., et al. 2012, MNRAS, 421, 284

Kennicutt, R., C., Jr., ARA&A, 36, 189

Kravtsov, A. V., Berlind, A. A., Wechsler, R. H., Klypin, A. A., Gottlöber, Stefan, Allgood, B., Primack, J. R., 2004, ApJ, 609, 35

Lagos, C. Del P., Lacey, C. G., Baugh, C. M., Bower, R. G., Benson, A. J., 2011, MNRAS, 416, 1566

Landy, S. D., & Szalay, A. S., ApJ, 412, 64

Leureijs, R., 2011, arXiv:1110.3193

Lawrence, A., et al., 2007, MNRAS, 379, 1599

Limber, N. D., 1954, APJ, 119, 655

Nakajima A., Shioya Y., Nagao T., Saito T., Murayam T., Sasaki S. S., Yokouchi A., Taniguchi Y., 2008, PASJ, 60, 1249

Navarro, J. F., Frenk, C. S., White, S. D. M., 1997, ApJ, 490, 493

Noeske, K. G, et al., 2007, ApJ, 660, 43

Norberg, P., et al, 2001, MNRAS, 328, 64

Norberg, P., Baugh, C. M., Gaztañaga, E., Croton, D. J., 2009, MNRAS, 396, 19

Matsuda, Y., et al., 2011, MNRAS, 416, 2041

Mo, H. J., White, S. D. M., 1996, MNRAS, 282, 347

Miller et al. 2004, MN, 355, 385

Myers, A. D., 2006, ApJ, 638, 622

Myers, A. D., Brunner, R. J., Nichol, R. C., Richards, G. T., Schneider, D. P., Bahcall, N. A., 2007, ApJ 658, 85

Orsi, A., Baugh, C. M., Lacey, C. G., Cimatti, A., Wang, Y., Zamorani, G., 2010, MNRAS, 405, 1006

Ouchi, M., et al., 2003, ApJ, 582, 60

Peebles, P. J. E., 1980, The large-scale structure of the universe, Research supported by the National Science Foundation. Princeton, N.J., Princeton University Press, 1980. 435 p.

Peebles, P. J. E., 1993, Principles of physical cosmology, Princeton University Press, Princeton, NJ

Prescott, M. K. M., Impey, C. D., Cool, R. J., Scoville, N. Z., 2006, ApJ, 644, 100

Quadri, R. F., Williams, R. J., Lee, K.-S., Franx, M., van Dokkum, P., Brammer, G. B., 2008, ApJ, 685, 1

Roche, N., Eales, S. A., Hippelein, H, Willott, C. J., 1999, MNRAS, 306, 538

Ross, N. P., et al., ApJ, 697, 1634

Rubin, V. C., 1954, Proceedings of the National Academy of Science, volume 40, 541–549

Scoville, N., et al., 2007, ApJS, 172, 1

Shao J., 1986, Ann. Stat., 14, 1322

Sheth, Ravi K., Mo, H. J., Tormen, Giuseppe, 2001, MNRAS, 323, 1

Shioya, Y., et al. ApJS, 175, 128

Simon, P., 2007, A&A, 473, 711

Smith, R. E., Peacock, J. A., Jenkins, A., White, S. D. M., Frenk, C. S., Pearce, F. R., Thomas, P. A., Efstathiou, G., Couchman, H. M. P., 2003, MNRAS, 341, 1311

Sobral, D., Smail, I., Best, P. N., Geach, J. E., Matsuda, Y., Stott, J. P., Cirasuolo, M., Kurk, J., 2012, 2012arXiv1202.3436S, MNRAS in press

Sobral, D., Best, P. N.; Smail, Ian; Geach, J. E.; Cirasuolo, M.; Garn, T.; Dalton, G. B., 2011, MNRAS, 411, 675

Sobral, D., Best, P. N., Geach, J. E., Smail, I., Cirasuolo, M., Garn, T., Dalton, G. B. Kurk, J., 2010, MNRAS, 404, 1551

Spitler, L. R., et al., 2012, ApJL, 748, L21

Springel, V., et al. 2005, Nature, 435, 629

Tinker, J., Kravtsov, A. V., Klypin, A., Abazajian, K., Warren, M., Yepes, G., Gottlöber, S., Holz, D. E., 2008, ApJ, 688, 709

Tinker, J. L., Robertson, B. E., Kravtsov, A. V., Klypin, A., Warren, A. S., Yepes, G., Gottlöber, S., 2010 ApJ, 724, 878

Wake, D. A., et al., 2008, MNRAS, 387, 1045

Wake, D. A., et al., 2011, ApJ, 728, 46

White, S. D. M., Rees, M. J., 1978, MNRAS, 183, 341

Yang, X., Mo, H. J., van den Bosch, F. C., 2003, MNRAS, 339, 1057

York, D., et al. 2000, AJ, 120, 1579

Zehavi, I., et al., 2011, ApJ, 736, 59

Zheng, Z., Berlind, A. A., Weinberg, D. H., Benson, A. J., Baugh, C. M., Cole, S., Davé, R., Frenk, C. S., Katz, N., Lacey, C. G., 2005, ApJ, 633, 791

Zheng, Z., Coil, A. L., Zehavi, I., 2007, ApJ, 667, 760